AIAA JOURNAL
Vol. 43, No. 5, May 2005

Accurate Spatial Resolution Estimates for Reactive Supersonic Flow with Detailed Chemistry

Joseph M. Powers* and Samuel Paolucci†
University of Notre Dame, Notre Dame, Indiana 46556-5637

A robust method is developed and used to provide rational estimates of reaction zone thicknesses in one-dimensional steady gas-phase detonations in mixtures of inviscid ideal reacting gases whose chemistry is described by detailed kinetics of the interactions of N molecular species constituted from L atomic elements. The conservation principles are cast as a set of algebraic relations giving pressure, temperature, density, velocity, and L species mass fractions as functions of the remaining N–L species mass fractions. These are used to recast the N–L species evolution equations as a self-contained system of nonlinear ordinary differential equations of the form $dY_i/dx = f_i(Y_1, \ldots, Y_{N-L})$. These equations are numerically integrated from a shock to an equilibrium end state. The eigenvalues of the Jacobian of f_i are calculated at every point in space, and their reciprocals give local estimates of all length scales. Application of the method to the standard problem of a stoichiometric Chapman–Jouguet hydrogen–air detonation in a mixture with ambient pressure of 1 atm and temperature of 298 K reveals that the finest length scale is on the order of 10^{-5} cm; this is orders of magnitude smaller than both the induction zone length, 10^{-2} cm, and the overall reaction zone length, 10^{0} cm. To achieve numerical stability and convergence of the solution at a rate consistent with the order of accuracy of the numerical method as the spatial grid is refined, it is shown that one must employ a grid with a finer spatial discretization than the smallest physical length scale. It is shown that published results of detonation structures predicted by models with detailed kinetics are typically underresolved by one to five orders of magnitude.

I. Introduction

In recent years there has been great interest in computations of complex multiscale physical phenomena. In this work, the simple issue of whether such computations have captured the breadth of length scales they purport to model is examined, and conditions are found under which such predictions are mathematically verifiable. The specific purpose of this paper is to give an accurate estimate of what spatial resolution is necessary for an important paradigm multiscale problem: gas-phase detonation described by detailed chemical kinetics. The general approach presented here can be extended to a wider range of problems, including those that are the subject of present intense computational investigations such as laminar flame propagation, supernova dynamics, combustion in reactive solids, flows in jet engines, and flows in rocket nozzles.

The ever-increasing capabilities of computational hardware and algorithms offer the scientific and engineering communities the opportunity to solve unsteady multidimensional problems that only a few years ago would have been impossible. However, this has necessitated a more complex interplay between mathematics, computation, and experiment; to determine via computation whether the underlying mathematical model is representative of the observable physics, one must first guarantee that the computations have fidelity with the underlying mathematics; this is sometimes defined as verification.[1–4] Only then is it appropriate to make comparisons with experiment, sometimes defined as validation, which, while critically important, will not be considered here. Neglecting the process of harmonizing computational predictions with the underlying mathematics, and, thus, simply tuning computational results with experiments, gives rise to the strong possibility that the predictions depend on both the size of the discrete grid and the particular algorithm used to solve the underlying equations.

Concerns regarding verification are typically minimal in problems for which the spatial and temporal scales over which the system evolves are nearly the same order of magnitude. In such cases, errors are usually obvious and easily corrected. However, in so-called multiscale problems, in which the range of spatiotemporal scales may span many orders of magnitude, verification is more difficult. In scenarios where the coupling across scales is weak, large-scale results, readily seen in predictions, may be relatively insensitive to errors at the small scales. In other problems, typically with stronger nonlinearities, the coupling across scales can be significant, and errors at the small scale can rapidly cascade to the large scale. Because for many problems it is difficult to obtain clear a priori information of the strength of this coupling, the only way one can gain confidence in predictions is to guarantee that all scales have been properly captured.

A prototypical multiscale example is found in gas-phase detonation with detailed chemistry. Over the past few decades, the aerospace propulsion community has utilized multiscale aerothermochemistry models of increasing complexity for sophisticated problems including flows in and around reentry vehicles, rocket nozzles, supersonic combustion ramjets, and pulse detonation wave engines. Because the geometries of these devices are on typical engineering scales and the chemistry typically evolves on a variety of significantly smaller length scales, it is clear that this is a multiscale problem. It must be said that in some problems, such as determination of detonation wave speeds and peak pressures, a posteriori calculations reveal only a weak dependence on properly capturing fine scale structures. However, other calculations, for instance, those of detonation instability or pollutant formation, can have a strong dependence on the fine structures. Whatever the case, it is not clear that the finest length scales have been resolved in most studies. Even in the most careful, it is rare to see a rigorous grid convergence study or an analysis that shows that the finest scales have been captured. To the contrary, it is more common to find the curious situation in which an argument is made for the necessity of a detailed kinetics model to capture the true physics of a problem, only to be followed by either 1) a rationalization as to why it is not necessary to have a fine grid

Received 17 June 2004; presented as Paper 2005-1171 at the 43rd Aerospace Sciences Meeting, Reno, NV, 10–13 January 2005; revision received 18 November 2004; accepted for publication 29 November 2004.

*Associate Professor, Department of Aerospace and Mechanical Engineering; powers@nd.edu. Associate Fellow AIAA.

†Professor, Department of Aerospace and Mechanical Engineering; paolucci@nd.edu.

capture the detailed physics or, more commonly, 2) no recognition that fine-scale physics has been overwhelmed by numerical errors.

To highlight this point, this study focuses on one key issue: determination of the finest length scale necessary to capture the smallest features present in a routinely used aerothermochemistry model of detonation. If calculations based on models of this class are to be able to withstand scientific scrutiny with regards to repeatability, grid- and algorithm-independence, consistent with AIAA standards for computations, they must, at a minimum, capture this finest scale. Even then, depending on the problem, there may be even finer length scales present, due to other effects, for example, high wave number instabilities[5] or multidimensionality.[6]

This study considers the issue of length scales by addressing a single paradigm problem: a one-dimensional steady Chapman–Jouguet (CJ) detonation in an inviscid stoichiometric hydrogen–air mixture whose chemistry is described by 9 species undergoing 19 reversible reactions. Whereas there is often controversy regarding parameter values in detailed kinetics models, especially for high molecular weight hydrocarbons, the detailed model for hydrogen oxidation is widely regarded as well understood, and parametric uncertainties are small.[7,8]

Initially, the mixture is taken to consist of diatomic hydrogen, oxygen, and nitrogen in the molar ratio of $2H_2 + O_2 + 3.76N_2$ at a pressure of 1 atm and temperature of 298 K. Nitrogen is modeled as an inert diluent. This is precisely the hydrogen–air problem studied by Shepherd,[9] who reported global reaction zone structures. It is closely related to the under-appreciated study of Mikolaitis,[10] who, following a general procedure used by Westbrook,[8] used the same kinetics model to give one of the most carefully resolved calculations of the temporal variation of all variables within what is known as the induction zone, that is, the early part of the reaction process in which pressure, temperature, and velocity are essentially constant and minor species mass fractions are rapidly growing. Shepherd's predictions of the variation of variables within the induction zone are difficult to discern in his plots. It will also be possible to compare to the recent results of Lu et al.,[11] who use a similar kinetics model to carefully predict induction zone lengths; however, they do not report the fine-scale details. In a somewhat similar calculation, Fickett and Davis[7] give a fully resolved prediction of a steady CJ detonation in $2H_2 + O_2 + 9Ar$ initially at 300 K and 0.1 atm; because the ambient pressure is lower, the reaction zone is larger.

Of those spatiotemporal studies that exercise care in resolving spatial structures, it is typically the induction zone length that is deemed to be the smallest length scale to be resolved. Such is the case in the studies of Oran et al.,[12] Hu et al.,[13] Eckett et al.,[14] Pintgen et al.,[15] Sheffer et al.,[16,17] Tsuboi et al.,[18] and da Silva et al.,[19] Nevertheless, because the thermal explosion at the end of the induction zone is the result of the cumulative nonlinear effects of reactions at finer scales, it is natural to suppose accurate prediction of the induction zone depends on accurate calculation of more primitive finer scale phenomena. The study of Singh et al.[20] has captured an even finer viscous scale. Their calculations, which took advantage of an adaptive spatial discretization method, came closest to resolving the finest reaction scales. Other studies have been less rigorous and give predictions in which it is unclear if even the induction zone has been resolved. Examples include those of Fedkiw et al.,[21] Ebrahimi and Merkle,[22] Dudebout et al.,[23] and Choi et al.[24] Recognizing the difficulties in resolving the finest scales of detailed kinetics, others take alternate approaches: 1) one-step kinetics, He and Karagozian,[25] or 2) two-step kinetics, Sichel et al.[26] or Kawai and Fujiwara,[27] based on the approach of Korobeinikov et al.[28] Both one- and two-step models require some compromises, described fully by the cited authors, in which the sacrifice of many terms results in a restricted ability to describe some physical phenomena relative to the detailed models. Moreover, even in two-step studies, the relative lengths of the individual reaction zone structures are not always clarified; if the smallest is not resolved, the same concerns one has for detailed kinetics models are realized. That is, a small number of reactions in no way guarantees the computation is made easier to perform accurately. In contrast, one could also have a system with hundreds of reactions, and if by chance they all evolved over a similar length scale, the computation could be done with both accuracy and efficiency.

The paper is organized as follows. First, a full description of the underlying unsteady reactive Euler equations is given. This is followed by details of the steps necessary to reduce the system to a set of ordinary differential equations (ODEs) describing the spatial evolution of a subset of the species mass fractions. Next, a standard linear analysis is performed to reveal that, at a given point in the reaction zone structure, the local length scales over which the system evolves are given by the reciprocal of the magnitude of the real part of each of the eigenvalues of the local Jacobian matrix of the nonlinear function on the right-hand side of the ODEs. This is followed by a description of the numerical method used to solve the system. Results are then shown for the spatial evolution of species mole fractions (used so that proper comparisons can be made with results in the literature), thermodynamic variables, and local length scales for the paradigm CJ detonation. A comparison of the finest scales to the induction zone length scales is given, followed by a study of accuracy and numerical stability. Then a summary of some recent predictions given in the literature of hydrogen–air, hydrogen–oxygen, and hydrogen–oxygen–argon detonations with detailed kinetics is given, and grid sizes used in those models are compared with the minimum physical length scale predicted by the present analysis. The implications of the results are reviewed in the concluding section.

II. Mathematical Model

A. Governing Equations

The following equations, written in unsteady conservative form, describe the behavior of a one-dimensional inviscid mixture of N gaseous molecular species composed of L atomic elements which undergo J reactions:

$$\frac{\partial \rho}{\partial t} + \frac{\partial}{\partial x}(\rho u) = 0 \tag{1}$$

$$\frac{\partial}{\partial t}(\rho u) + \frac{\partial}{\partial x}(\rho u^2 + p) = 0 \tag{2}$$

$$\frac{\partial}{\partial t}\left[\rho\left(e + \frac{u^2}{2}\right)\right] + \frac{\partial}{\partial x}\left[\rho u\left(e + \frac{u^2}{2} + \frac{p}{\rho}\right)\right] = 0 \tag{3}$$

$$\frac{\partial}{\partial t}(\rho Y_i) + \frac{\partial}{\partial x}(\rho u Y_i) = \dot{\omega}_i M_i, \qquad i = 1, \ldots, N-1 \tag{4}$$

The independent variables are the distance coordinate x and time t. The dependent variables are density ρ, velocity u, pressure p, specific internal energy e, species mass fractions $Y_i, i = 1, \ldots, N-1$, and molar production rate per unit volume for specie i, $\dot{\omega}_i, i = 1, \ldots, N-1$. The parameters are the molecular masses of specie i, $M_i, i = 1, \ldots, N-1$. Equations (1–3) describe the conservation of mixture mass, linear momentum, and energy, respectively. Equation (4) describes the evolution of $N-1$ of the molecular species mass fractions.

The system is completed by the following algebraic equations:

$$p = \rho \Re T \sum_{i=1}^{N} \frac{Y_i}{M_i} \tag{5}$$

$$e = \sum_{i=1}^{N} Y_i \left(h_i^0 - \frac{\Re T}{M_i}\right) \tag{6}$$

$$1 = \sum_{i=1}^{N} Y_i \tag{7}$$

$$\dot{\omega}_i = \sum_{j=1}^{J} \nu_{ij} r_j, \qquad i = 1, \ldots, N-1 \tag{8}$$

$$r_j = A_j T^{\beta_j} \exp\left(\frac{-E_j}{\Re T}\right)\left(\underbrace{\prod_{k=1}^{N}\left(\frac{\rho Y_k}{M_k}\right)^{\nu'_{kj}}}_{\text{forward}} - \underbrace{\frac{1}{K_j^c}\prod_{k=1}^{N}\left(\frac{\rho Y_k}{M_k}\right)^{\nu''_{kj}}}_{\text{reverse}}\right) \qquad j = 1, \ldots, J \quad (9)$$

$$K_j^c = \left(\frac{p^{\text{ref}}}{\Re T}\right)^{\sum_{m=1}^{N}\nu_{mj}} \exp\left(\frac{-\sum_{m=1}^{N}\bar{\mu}_m^0 \nu_{mj}}{\Re T}\right), \qquad j = 1, \ldots, J \quad (10)$$

$$h_i^0 = h_i^{\text{ref}} + \int_{T^{\text{ref}}}^{T} c_{pi}(\hat{T})\,\mathrm{d}\hat{T}, \qquad i = 1, \ldots, N \quad (11)$$

$$s_i^0 = s_i^{\text{ref}} + \int_{T^{\text{ref}}}^{T} \frac{c_{pi}(\hat{T})}{\hat{T}}\,\mathrm{d}\hat{T}, \qquad i = 1, \ldots, N \quad (12)$$

$$\bar{\mu}_i^0 = M_i\left(h_i^0 - T s_i^0\right), \qquad i = 1, \ldots, N \quad (13)$$

$$M_i = \sum_{l=1}^{L} m_l \phi_{li}, \qquad i = 1, \ldots, N \quad (14)$$

$$0 = \sum_{i=1}^{N} \phi_{li}\nu_{ij}, \qquad j = 1, \ldots, J, \qquad l = 1, \ldots, L \quad (15)$$

$$\nu_{ij} = \nu''_{ij} - \nu'_{ij}, \qquad i = 1, \ldots, N, \qquad j = 1, \ldots, J \quad (16)$$

New dependent variables are the temperature T; the specific heat at constant pressure of the ith specie, c_{pi}, taken to be a function of temperature, where $\hat{T}$ is a dummy variable of integration; the mass fraction of the Nth specie Y_N; the reaction rate of the jth reaction r_j; and the so-called equilibrium constant of the jth reaction, K_j^c. Also, a set of new variables for ith specie, denoted with a superscript 0 to indicate evaluation at the reference pressure, are defined as the chemical potential per unit mole, enthalpy per unit mass, and entropy per unit mass, $\bar{\mu}_i^0, h_i^0$, and s_i^0, respectively. The bar notation indicates a per mole basis.

Parameters in Eqs. (5–15) are as follows. The universal gas constant is $\Re$. The pressure and temperature at the reference state are p^{ref} and T^{ref}, respectively. For each molecular specie from $i = 1, \ldots, N$, one has reference state specific enthalpy and entropy, h_i^{ref} and s_i^{ref}. For each reaction $j = 1, \ldots, J$, one has collision frequency factor A_j, exponent characterizing power-law temperature dependency, β_j, activation energy E_j, and stoichiometric coefficients denoting the number of moles of reactant and product, respectively, of specie i in reaction j, ν'_{ij} and ν''_{ij}, as well as the net stoichiometric coefficients ν_{ij}. For $l = 1, \ldots, L$, the atomic element mass is m_l. For specie $i = 1, \ldots, N$, and atomic element $l = 1, \ldots, L$, the species atomic element index giving number of moles of atomic element l in specie i is ϕ_{li}.

Equation (5) is a thermal equation of state for a mixture of ideal gases, which obeys Dalton's law. Equation (6) is a mixing rule for the internal energy. Equation (7) constrains the species mass fractions to sum to unity. Equation (8) is an expression for the molar species evolution rate per unit volume for specie i. Equation (9) is an expression of the law of mass action with Arrhenius kinetics for reaction j constructed so as to ensure the forward and reverse reaction rate components satisfy Le Châtlier's principle as each individual reaction approaches equilibrium. Equation (10) is an equation for the equilibrium constant for each reaction; actually K_j^c is a function of T. Equations (11–13) define the enthalpy, entropy, and chemical potential of specie i, evaluated at p^{ref}, as functions of temperature. The variables $h_i^0(T)$ and $s_i^0(T)$ are often available in tabular form; alternatively, functional forms for $c_{pi}(T)$ may be available. Equation (14) defines the molecular mass in terms of its constitutive atomic elements. Equation (15) is a stoichiometric constraint on atomic element l in reaction j. After use of Eqs. (8–13) to eliminate $\dot{\omega}_i$ in Eq. (4), Eqs. (1–7) form $5 + N$ equations in the $5 + N$ unknowns, ρ, u, p, e, T, and $Y_1, \ldots, Y_N$.

A nonobvious identity is obtained by operating on the N-term version of Eq. (4). One notes that by summing Eq. (4) from $i = 1$ to N and employing Eqs. (8), (14), and (15), one arrives at

$$\frac{\partial}{\partial t}\left(\rho \sum_{i=1}^{N} Y_i\right) + \frac{\partial}{\partial x}\left(\rho u \sum_{i=1}^{N} Y_i\right) = \sum_{j=1}^{J} r_j \sum_{l=1}^{L} m_l \underbrace{\sum_{i=1}^{N} \phi_{li}\nu_{ij}}_{=0} = 0 \quad (17)$$

Using next Eq. (7) to eliminate the sum of mass fractions in Eq. (17), one finds consistency with Eq. (1).

Additional useful auxiliary equations are as follows:

$$y_l = m_l \sum_{i=1}^{N} \frac{\phi_{li}}{M_i} Y_i, \qquad l = 1, \ldots, L \quad (18)$$

$$X_i = \frac{Y_i/M_i}{\sum_{j=1}^{N} Y_j/M_j}, \qquad i = 1, \ldots, N \quad (19)$$

$$c_{vi} = c_{pi} - \frac{\Re}{M_i}, \qquad i = 1, \ldots, N \quad (20)$$

$$c_p = \sum_{i=1}^{N} Y_i c_{pi} \quad (21)$$

$$c_v = \sum_{i=1}^{N} Y_i c_{vi} \quad (22)$$

$$\gamma = \frac{c_p}{c_v} \quad (23)$$

$$c = \sqrt{\gamma \frac{p}{\rho}} \quad (24)$$

$$M = \frac{u}{c} \quad (25)$$

$$p_i = \rho \Re T \frac{Y_i}{M_i}, \qquad i = 1, \ldots, N \quad (26)$$

$$h_i = h_i^0 \quad (27)$$

$$s_i = s_i^0 - \frac{\Re}{M_i}\,\ell_n\left(\frac{p_i}{p^{\text{ref}}}\right), \qquad i = 1, \ldots, N \quad (28)$$

$$\bar{\mu}_i = \bar{\mu}_i^0 + \Re T\,\ell_n\left(\frac{p_i}{p^{\text{ref}}}\right) = \bar{g}_i = M_i(h_i - T s_i), \qquad i = 1, \ldots, N \quad (29)$$

$$1 = \sum_{l=1}^{L} y_l \quad (30)$$

New dependent variables in Eqs. (18–30) are as follows. For each atomic element $l = 1, \ldots, L$, one has the element mass fraction y_l. For each molecular specie, $i = 1, \ldots, N$, one has the mole fraction X_i, the specific heat at constant volume c_{vi}, the partial pressure p_i, and the Gibbs free-energy per mole $\bar{g}_i$. One has the mass-averaged specific heats at constant pressure and volume, respectively, c_p and c_v, the ratio of specific heats γ, the frozen acoustic speed c, and the Mach number M. Equations (18–29) are definitions of y_l, X_i, c_{vi}, $c_p, c_v, \gamma, c, M, p_i, h_i, s_i, \bar{\mu}_i$, and $\bar{g}_i$, respectively. For the ideal gas, h_i is a function of temperature alone; however, both s_i and $\bar{\mu}_i$ are functions of temperature and pressure. Last, Eq. (30) constrains the

atomic element mass fractions and can be derived from summing Eq. (18) from $l = 1$ to L and employing Eq. (14).

It is easily shown, using techniques described by Whitham,[29] that Eqs. (1–7) form a hyperbolic system and, thus, admit propagating discontinuous jumps. For a stationary jump at $x = 0$, which will be considered here, the equations reduce to

$$[\![\rho u]\!] = 0 \tag{31}$$

$$[\![\rho u^2 + p]\!] = 0 \tag{32}$$

$$[\![\rho u(e + u^2/2 + p/\rho)]\!] = 0 \tag{33}$$

$$[\![\rho u Y_i]\!] = 0, \qquad i = 1, \ldots, N \tag{34}$$

Here, a common variant of Whitham's notation for a shock jump has been employed: $[\![\Psi]\!] \equiv \Psi|_{x=0^+} - \Psi|_{x=0^-}$, where Ψ is a generic quantity. Substitution of Eq. (31) into Eq. (34) gives the standard result that species mass fractions are frozen through a discontinuity: $[\![Y_i]\!] = 0$, $i = 1, \ldots, N$. As a consequence, Eqs. (31–33) combined with Eqs. (5) and (6) form a set of five algebraic equations in the five unknowns ρ, u, p, e, and T, which can be shown to admit two physical solutions: the ambient state and the shock state.

The driving inhomogeneity of the system is the term $\dot{\omega}_i$ in Eq. (4). Examination of Eq. (9) reveals that r_j is driven to zero when

$$K_j^c(T) = \prod_{k=1}^{N} \left(\frac{\rho Y_k}{M_k}\right)^{\nu_{kj}}, \qquad j = 1, \ldots, J \tag{35}$$

Driving r_j, $j = 1, \ldots, J$, to zero is sufficient to drive $\dot{\omega}_i$, $i = 1, \ldots, N$, to zero. To show it is necessary requires significantly more effort. A lengthy, but standard, analysis of Eq. (35) utilizing Eqs. (10–13) and (26–29) reveals the sufficient equilibrium condition to be equivalent to

$$\sum_{i=1}^{N} \bar{\mu}_i \nu_{ij} = 0, \qquad j = 1, \ldots, J \tag{36}$$

which can be shown to correspond to minimization of the Gibbs free energy.

B. Reduction of System

The assumptions and operations necessary to reduce the system to N–L ODEs in N–L unknowns are given next. For each atomic element $l = 1, \ldots, L$, multiply each side of Eq. (4) by the constant term $m_l \phi_{il}/M_i$, sum the result from $i = 1$ to N, and employ Eqs. (15) and (18) to obtain

$$\frac{\partial}{\partial t}(\rho y_l) + \frac{\partial}{\partial x}(\rho u y_l) = 0, \qquad l = 1, \ldots, L \tag{37}$$

This demonstrates that the mass of each atomic element is conserved. Moreover, when Eq. (37) is combined with Eq. (1), one finds that

$$\frac{\partial y_l}{\partial t} + u\frac{\partial y_l}{\partial x} = 0, \qquad l = 1, \ldots, L \tag{38}$$

That is, for a material fluid particle, there is no time rate of change of atomic element mass fraction. Consequently, atomic element mass fraction distributions in mixtures that are initially spatially homogeneous remain homogeneous. This study will be concerned only with such mixtures; consequently,

$$y_l(x, t) = y_{l0}, \qquad l = 1, \ldots, L \tag{39}$$

where the initial value of atomic element mass fractions y_{l0} can be fixed from initial conditions, which, from Eq. (30), are constrained so that

$$\sum_{l=1}^{L} y_{l0} = 1$$

Here, the subscript 0 represents the ambient state. Thus, one can apply this result to cast Eq. (18) as an underconstrained system of L linear equations in N unknowns ($L < N$):

$$y_{l0} = m_l \sum_{i=1}^{N} \frac{\phi_{li}}{M_i} Y_i, \qquad l = 1, \ldots, L \tag{40}$$

Equation (40) can be rewritten into a variety of consistent row-echelon forms. Assuming the variables are ordered such that the last L entries for Y_i have nonzero pivots, one can invert Eq. (40) to obtain

$$Y_{N-l+1} = \psi_l[Y_1, \ldots, Y_{N-L}; y_{l0}, (\phi_{l1}/M_1), \ldots, (\phi_{lN}/M_N)] \qquad l = 1, \ldots, L \tag{41}$$

Here ψ_l is a linear function of the first N–L species mass fractions, parameterized by the atomic element mass fractions, molecular masses, and species atomic element indices. As a result, it is possible to replace the N equations given by Eq. (4), $i = 1, \ldots, N-1$, and Eq. (7) by the N equations given by Eq. (4), $i = 1, \ldots, N$–L, and Eq. (41), $l = 1, \ldots, L$.

It is now assumed that a stationary solution exists so that Eqs. (1–3) and the first N–L of Eqs. (4) become the following ODEs in the spatial independent variable x, which is now considered to be a wave-attached coordinate:

$$\frac{\mathrm{d}}{\mathrm{d}x}(\rho u) = 0 \tag{42}$$

$$\frac{\mathrm{d}}{\mathrm{d}x}(\rho u^2 + p) = 0 \tag{43}$$

$$\frac{\mathrm{d}}{\mathrm{d}x}\left[\rho u\left(e + \frac{u^2}{2} + \frac{p}{\rho}\right)\right] = 0 \tag{44}$$

$$\frac{\mathrm{d}}{\mathrm{d}x}(\rho u Y_i) = \dot{\omega}_i M_i, \qquad i = 1, \ldots, N\text{–}L \tag{45}$$

Initial conditions are specified so that just before the shock jump at $x = 0^-$ one has

$$\rho(0^-) = \rho_0, \qquad u(0^-) = D, \qquad p(0^-) = p_0, \qquad Y_i(0^-) = Y_{i0} \qquad i = 1, \ldots, N\text{–}L \tag{46}$$

Here, D represents the ambient fluid velocity. Then, using Eqs. (46) with Eqs. (5) and (6), one can find consistent values for

$$e(0^-) = e_0, \qquad T(0^-) = T_0 \tag{47}$$

The homogeneous Eqs. (42–44) can then be integrated to obtain extended Rankine–Hugoniot equations, and Eq. (45) can be simplified to obtain

$$\rho u = \rho_0 D \tag{48}$$

$$\rho u^2 + p = \rho_0 D^2 + p_0 \tag{49}$$

$$e + \frac{u^2}{2} + \frac{p}{\rho} = e_0 + \frac{D^2}{2} + \frac{p_0}{\rho_0} \tag{50}$$

$$\frac{\mathrm{d}Y_i}{\mathrm{d}x} = \frac{\dot{\omega}_i M_i}{\rho_0 D}, \qquad i = 1, \ldots, N\text{–}L \tag{51}$$

After defining the intermediate function $\sigma(Y_i)$ as

$$\sigma(Y_i) \equiv \sum_{i=1}^{N} \frac{Y_i}{M_i} \tag{52}$$

a detailed algebraic analysis of Eqs. (5), (48), and (49) allows one to formulate an explicit expression for $\rho(T, Y_i)$:

$$\rho(T, Y_i) = \rho_0 \frac{D^2}{2\Re T\sigma(Y_i)} \times \left\{ 1 + \frac{\Re T_0\sigma(Y_{i0})}{D^2} \pm \sqrt{\left[1 + \frac{\Re T_0\sigma(Y_{i0})}{D^2}\right]^2 - 4\frac{\Re T\sigma(Y_i)}{D^2}} \right\} \tag{53}$$

The + and − branches are associated with perturbations from the shock and inert states, respectively. Combining Eq. (53) with Eq. (48) gives $u(T, Y_i)$. Then, Eq. (49) can be used to obtain $p(T, Y_i)$, followed by use of Eq. (50) to get $e(T, Y_i)$. Combining the expression for $e(T, Y_i)$ with Eq. (6) as well as employing Eq. (41) yields an implicit algebraic relation between T and Y_i, $i = 1, \ldots, N\text{–}L$:

$$\sum_{i=1}^{N} Y_i \left[h_i^{\mathrm{ref}} + \int_{T^{\mathrm{ref}}}^{T} c_{pi}(\hat{T})\, \mathrm{d}\hat{T} - \frac{\Re T}{M_i} \right] - e_0 + \frac{\Re T\sigma(Y_i)}{2} - \frac{\Re T_0\sigma(Y_{i0})}{2}\left[1 - \frac{\Re T_0\sigma(Y_{i0})}{2D^2}\right] - \frac{D^2}{4}\left\{ 1 \pm \left[1 + \frac{\Re T_0\sigma(Y_{i0})}{D^2}\right] \times \sqrt{\left[1 + \frac{\Re T_0\sigma(Y_{i0})}{D^2}\right]^2 - 4\frac{\Re T\sigma(Y_i)}{D^2}} \right\} = 0 \tag{54}$$

One can use Newton iteration on Eq. (54) to determine $T(Y_i)$. Thus, for given Y_i, one gets T and then ρ, u, p, and e.

This study will deal exclusively with the shock (+) branch and will consider the fixed shock to be located at $x = 0$. A fluid particle approaching from $x < 0$ encounters the shock, decelerates, and proceeds at a slower speed in the direction of increasing x. If one were to apply a Galilean transformation to this system with frame velocity D, it is clear that this also describes a wave traveling at speed D in the direction of decreasing x into a fluid at rest. Thus one can interpret D as the classical detonation wave speed. Also, it is easily determined that the critical value of D^2 is given by

$$D^2 = \Re T_0\sigma(Y_{i0}) \left\{ \left[2\frac{T\sigma(Y_i)}{T_0\sigma(Y_{i0})} - 1 \right] \pm \sqrt{\left[2\frac{T\sigma(Y_i)}{T_0\sigma(Y_{i0})} - 1 \right]^2 - 1} \right\} \tag{55}$$

Here the + and − branches are for detonations and deflagrations, respectively. On the detonation branch, no real solution exists for values of D^2 below the critical value. Correspondingly, on the deflagration branch, no real solution exists for values of D^2 above the critical value. Note that Eq. (55) does not explicitly give the most useful extended CJ condition because it remains a function of T. An explicit determination of an extended CJ condition could be found if Eq. (54) could be explicitly solved for T.

Endowed with effective representations of dependent variables in terms of the $N\text{–}L$ species mass fractions, one can then use Eq. (8) to obtain $\dot{\omega}_i(Y_1, \ldots, Y_{N-L})$. In the same way, one obtains all auxiliary variables in Eqs. (18–30) as functions of $Y_1, \ldots, Y_{N-L}$. Consequently, it is possible to write Eq. (51) and the relevant part of Eq. (46) as a set of nonlinear ODEs and initial conditions in the standard form,

$$\frac{\mathrm{d}Y_i}{\mathrm{d}x} = f_i(Y_1, \ldots, Y_{N-L}), \qquad Y_i(0^-) = Y_{i0}, \qquad i = 1, \ldots, N\text{–}L \tag{56}$$

where f_i is a nonlinear function of the dependent variables given by $f_i = \dot{\omega}_i M_i/(\rho_0 D)$. Except for certain special cases, for example, reactions that each preserve the number of molecules so that more conserved variables exist, in general, Eqs. (56) are the minimal set necessary to describe the steady spatial structure of a gas-phase detonation in a system which is described by detailed kinetics.

C. Length Scale Analysis

One can apply a standard eigenvalue analysis to Eqs. (56) to accurately estimate the local length scales over which the system evolves. Define, for convenience, the column vector $\boldsymbol{y} = Y_i$, $i = 1, \ldots, N\text{–}L$, and consider a point $x = x^*$ at which $\boldsymbol{y} = \boldsymbol{y}^*$, which may or may not be near an equilibrium state. Assuming that the local Jacobian matrix of f_i, taken to be $\boldsymbol{J} = \partial f_i/\partial Y_j|_{y=y^*}$, is nonsingular, one can linearize Eq. (56) to arrive at

$$\frac{\mathrm{d}\boldsymbol{y}}{\mathrm{d}x} = \boldsymbol{J} \cdot (\boldsymbol{y} - \boldsymbol{y}^*) + \boldsymbol{b}, \qquad \boldsymbol{y}(x^*) = \boldsymbol{y}^* \tag{57}$$

Here, $\boldsymbol{b}$ is a constant column vector of dimension $N\text{–}L$, and $\boldsymbol{J}$ has dimension $(N\text{–}L) \times (N\text{–}L)$. When $\boldsymbol{b} = \boldsymbol{0}$, the state $\boldsymbol{y} = \boldsymbol{y}^*$ corresponds to an equilibrium state. As described by Fickett and Davis,[7] one can expect singular behavior near sonic points. Extreme care must be exercised in such circumstances; it is often the case that detailed kinetics can induce the true propagation speed of an unsupported detonation to deviate from that given by a classical CJ analysis. To avoid such concerns, this study only considers waves that are traveling slightly faster than the CJ speed, which physically suggests the presence of weak piston support.

Next, define a new dependent variable $\boldsymbol{z}$ such that

$$\boldsymbol{z} = \boldsymbol{y} - \boldsymbol{y}^* + \boldsymbol{J}^{-1} \cdot \boldsymbol{b} \tag{58}$$

Eliminating $\boldsymbol{y}$ from Eq. (57) in favor of $\boldsymbol{z}$, one gets

$$\frac{\mathrm{d}\boldsymbol{z}}{\mathrm{d}x} = \boldsymbol{J} \cdot \boldsymbol{z}, \qquad \boldsymbol{z}(x^*) = \boldsymbol{J}^{-1} \cdot \boldsymbol{b} \tag{59}$$

Assuming that $\boldsymbol{J}$ has a complete set of $N\text{–}L$ linearly independent eigenvectors, one can decompose $\boldsymbol{J}$ as $\boldsymbol{J} = \boldsymbol{P} \cdot \boldsymbol{\Lambda} \cdot \boldsymbol{P}^{-1}$, where $\boldsymbol{P}$ is the matrix whose columns are populated by the right eigenvectors of $\boldsymbol{J}$ and $\boldsymbol{\Lambda}$ is the diagonal matrix whose diagonal is composed of the eigenvalues λ_i, $i = 1, \ldots, N\text{–}L$, of $\boldsymbol{J}$. If an insufficient number of linearly independent eigenvectors are available, a Jordan decomposition can be used to obtain an equivalent result. Thus, Eq. (59) can be written as

$$\frac{\mathrm{d}\boldsymbol{z}}{\mathrm{d}x} = \boldsymbol{P} \cdot \boldsymbol{\Lambda} \cdot \boldsymbol{P}^{-1} \cdot \boldsymbol{z}, \qquad \boldsymbol{z}(x^*) = \boldsymbol{J}^{-1} \cdot \boldsymbol{b} \tag{60}$$

When the locally constant matrix operator $\boldsymbol{P}^{-1}$ is applied to both sides and $\boldsymbol{w} = \boldsymbol{P}^{-1} \cdot \boldsymbol{z}$ is defined, Eq. (60) transforms to the uncoupled set of equations

$$\frac{\mathrm{d}\boldsymbol{w}}{\mathrm{d}x} = \boldsymbol{\Lambda} \cdot \boldsymbol{w}, \qquad \boldsymbol{w}(x^*) = \boldsymbol{P}^{-1} \cdot \boldsymbol{J}^{-1} \cdot \boldsymbol{b} \tag{61}$$

Their solutions are

$$\boldsymbol{w}(x) = e^{\Lambda(x - x^*)} \cdot \boldsymbol{P}^{-1} \cdot \boldsymbol{J}^{-1} \cdot \boldsymbol{b} \tag{62}$$

The convenient matrix exponential notation has been utilized, which is described in many standard texts, for example, that of Strang.[30] Obviously, the ith component of $\boldsymbol{w}$ evolves on a local length scale ℓ_i given by

$$\ell_i = 1/|\mathrm{Re}(\lambda_i)|, \qquad i = 1, \ldots, N\text{–}L \tag{63}$$

This is the key result that will give the local length scales at all points in the reaction zone up to and including the equilibrium point. In the bulk of the detonation reaction zone structure, the eigenvalues are purely real. For the limited regions in which they are complex, the real part gives the length scale of amplitude growth, and the imaginary part gives an additional length scale of oscillation.

It is generally impossible to associate the evolution of a particular specie with a particular eigenvalue because the species mass fractions depend on local linear combinations of all components of $\boldsymbol{w}$ and, thus, include evolution on all of the $N\text{–}L$ length scales of the system. This is seen by reconstructing $\boldsymbol{y}$, from which one finds that the local evolution of the species mass fractions is described by

$$\boldsymbol{y}(x) = \boldsymbol{y}^* + \left(\boldsymbol{P} \cdot e^{\Lambda(x - x^*)} \cdot \boldsymbol{P}^{-1} - \boldsymbol{I} \right) \cdot \boldsymbol{J}^{-1} \cdot \boldsymbol{b} \tag{64}$$

Because this analysis is local, the eigenvalues, and, thus, the length scales, will vary with x; that is, one has $\lambda_i(x)$ and $\ell_i(x)$ throughout the reaction zone.

The analysis of this section gives the framework for a local description of the evolution of a finite set of chemical length scales, fixed by kinetic rates and satisfaction of conservation properties. As an aside, one can ask how the presence of additional mechanisms such as diffusion and unsteadiness would influence the local length scales. In the one-dimensional steady limit, each additional diffusion mechanism, for example, species, momentum, energy, adds a single ODE to the set and, thus, a new length scale. This could easily be analyzed in the manner already presented.

The addition of unsteadiness is more complicated because such a system is described by a set of partial differential equations (PDEs). In terms of the analysis of this section, one may consider the system of PDEs to be, after spatial discretization, a very large set of ODEs in time. A related eigenvalue analysis could be performed on the system's Jacobian, and a set of local timescales of evolution is available at each point in time. These timescales would exhibit, in general, full coupling between reaction, convection, and diffusion. In fact, one can show in the limit as the spatial discretization approaches zero that most timescales become increasingly dominated by diffusion and that the minimum timescale is on the order of the square of the spatial discretization size. For the error in an unsteady calculation, which includes diffusion to be converging to zero, one must have a discretization fine enough to render the diffusive timescales finer than the chemical timescales. This poses a serious computational challenge for most physically important problems.

III. Computational Method

All calculations were performed on a single processor Sun Blade 1000 with a speed of 900 MHz. Typical calculations were completed within 2 min. A double precision FORTRAN 90 code that drew on standard Integrated Mathematics and Statistics Library (IMSL) routines DNEQNF for Newton iteration, DFDJAC for Jacobian evaluation, and DEVLRG for eigenvalue computation was used. For evaluation of thermochemical properties, subroutines available in a double-precision version of the public domain edition of the Chemkin[31] package were utilized; no other general Chemkin tools for solving specific physical problems were employed. This package draws on a standard thermodynamic database[32] that contains properties for a wide variety of constituents; these include coefficients for polynomial curve fits for the variation of specific heats with temperature.

For integration, three methods were used: 1) a first-order explicit Euler method, 2) a second-order explicit Runge–Kutta method, and 3) an implicit Adams method with functional iteration as embodied in the standard code DLSODE[33] in which step sizes were adapted to achieve a user-defined absolute error tolerance, here taken as 10^{-14}. When all methods were run with a spatial discretization smaller than the smallest physical length scale, the predictions were virtually indistinguishable. The explicit Euler and Runge–Kutta codes utilized a constant spatial discretization step size, which was useful in grid convergence and numerical stability studies. The implicit Adams method was used in studies to obtain the complete reaction zone structure; here it was straightforward to adjust the spatial discretization step to generate detailed results in the induction zone and coarser results near equilibrium. However, even near equilibrium, it was seen that the number of internal steps taken to achieve the error tolerance was consistent with the discretization at the spatial scale dictated by the finest physical scale.

IV. Results

Results are presented for hydrogen–air mixtures, which are initially in a stoichiometric molar ratio of $2H_2 + O_2 + 3.76N_2$. A kinetic model with $N = 9$ species, $L = 3$ atomic elements, and $J = 19$ reversible reactions, identical to that employed by Shepherd[9] in his hydrogen–air calculations, is used and is reported in detail in Table 1. In Table 1, units of A_j are in appropriate combinations of centimeter, mole, second, and degrees Kelvin so that $\dot{\omega}_i$ has units of mole per cubic centimeter per second; units of E_j are calorie per mole. Third-body collision efficiencies with M are $k_5(H_2O) = 21$, $k_5(H_2) = 3.3$, $k_{12}(H_2O) = 6$, $k_{12}(H) = 2$, $k_{12}(H_2) = 3$, and $k_{14}(H_2O) = 20$. Obviously, there are many slightly different kinetic models from which to choose, and the differences in each may become apparent in sensitive regions of the reaction zone structure. However, analyzing the differences among the various kinetic models is beyond the scope of this study. The nine species modeled are H, O, H_2, O_2, OH, H_2O, HO_2, H_2O_2, and N_2. Diatomic nitrogen is regarded as an inert diluent. The three atomic elements are H, O, and N. Shepherd extracts this model from the more general model reported by Miller et al.[34] The kinetic model is nearly identical to that reported by Mikolaitis,[10] who has an obvious transcription error in his value for A_4. As use of this reported value has catastrophic consequences for the calculation, and Mikolaitis's results agree with Shepherd's and those of this study, it is likely that the correct value for A_4 was actually used in Ref. 10.

Table 1 Nine-species, 19-step reversible reaction mechanism for hydrogen/oxygen/nitrogen mixture[a]

j	Reaction	A_j	β_j	E_j
1	$H_2 + O_2 \rightleftharpoons OH + OH$	1.70×10^{13}	0.00	47,780
2	$OH + H_2 \rightleftharpoons H_2O + H$	1.17×10^{9}	1.30	3,626
3	$H + O_2 \rightleftharpoons OH + O$	5.13×10^{16}	−0.82	16,507
4	$O + H_2 \rightleftharpoons OH + H$	1.80×10^{10}	1.00	8,826
5	$H + O_2 + M \rightleftharpoons HO_2 + M$	2.10×10^{18}	−1.00	0
6	$H + O_2 + O_2 \rightleftharpoons HO_2 + O_2$	6.70×10^{19}	−1.42	0
7	$H + O_2 + N_2 \rightleftharpoons HO_2 + N_2$	6.70×10^{19}	−1.42	0
8	$OH + HO_2 \rightleftharpoons H_2O + O_2$	5.00×10^{13}	0.00	1,000
9	$H + HO_2 \rightleftharpoons OH + OH$	2.50×10^{14}	0.00	1,900
10	$O + HO_2 \rightleftharpoons O_2 + OH$	4.80×10^{13}	0.00	1,000
11	$OH + OH \rightleftharpoons O + H_2O$	6.00×10^{8}	1.30	0
12	$H_2 + M \rightleftharpoons H + H + M$	2.23×10^{12}	0.50	92,600
13	$O_2 + M \rightleftharpoons O + O + M$	1.85×10^{11}	0.50	95,560
14	$H + OH + M \rightleftharpoons H_2O + M$	7.50×10^{23}	−2.60	0
15	$H + HO_2 \rightleftharpoons H_2 + O_2$	2.50×10^{13}	0.00	700
16	$HO_2 + HO_2 \rightleftharpoons H_2O_2 + O_2$	2.00×10^{12}	0.00	0
17	$H_2O_2 + M \rightleftharpoons OH + OH + M$	1.30×10^{17}	0.00	45,500
18	$H_2O_2 + H \rightleftharpoons HO_2 + H_2$	1.60×10^{12}	0.00	3,800
19	$H_2O_2 + OH \rightleftharpoons H_2O + HO_2$	1.00×10^{13}	0.00	1,800

[a]Extracted from Ref. 34 and used in Refs. 9 and 10.

A. Stoichiometric CJ Hydrogen–Air Detonation at Standard Conditions

The model was used on a mixture, which in its unshocked state was at $p_0 = 1$ atm and $T_0 = 298$ K, under near-CJ conditions, taken as the state in which the Mach number at the equilibrium state approaches unity. The CJ state was determined by iteration and was found to be extremely sensitive to the initial velocity D; for this case $D \sim D_{CJ} \sim 1.9797 \times 10^5$ cm/s, giving rise to a freestream Mach number of 4.8594. As the resulting length scales were relatively insensitive to D, a final state with a Mach number slightly less than unity was tolerated, $M = 0.93824$. Also note, for detonations with resolved reaction zone structures, that it has been shown by Fickett and Davis[7] that the CJ state is the unique propagation speed of an unsupported detonation only for systems that employ simple kinetic schemes that are strictly irreversible and exothermic. For variants, such as reversible reactions or reactions with some endothermicity, the propagation speed of an unsupported detonation deviates from the CJ speed, and it is appropriate to consider so-called eigenvalue detonation speeds, which are often on the weak branch of the Hugoniot curve. Though not fully explored, during the iteration process employed here, calculations occasionally reached sonic points at states of incomplete reaction, which suggests that consideration should be given to the eigenvalue character of the detonation wave speed. Because the effects of reversibility are only strongly felt in the present system as it approaches equilibrium, and those of local endothermicity are weak, it is reasonable to expect the deviation from CJ state to be small.

Table 2 Thermochemical and dynamic properties for a mixture of $2H_2 + O_2 + 3.76N_2$

Property	Initial	Shock	CJ
p, atm	1.0000×10^{0}	2.7953×10^{1}	1.6267×10^{1}
T, K	2.9800×10^{2}	1.5427×10^{3}	2.9821×10^{3}
u, cm/s	1.9797×10^{5}	3.6661×10^{4}	1.0660×10^{5}
ρ, g/cm^3	8.5521×10^{-4}	4.6180×10^{-3}	1.5882×10^{-3}
e, erg/g	-1.1862×10^{9}	1.2789×10^{10}	3.5345×10^{9}
c_p, (erg/g)/K	1.3894×10^{7}	1.6485×10^{7}	1.7744×10^{7}
c_v, (erg/g)/K	9.9182×10^{6}	1.2509×10^{7}	1.4264×10^{7}
γ	1.4009×10^{0}	1.3178×10^{0}	1.2440×10^{0}
c, cm/s	4.0740×10^{4}	8.9904×10^{4}	1.1362×10^{5}
M	4.8594×10^{0}	4.0779×10^{-1}	9.3823×10^{-1}
Y_{O_2}	2.2636×10^{-1}	2.2636×10^{-1}	1.3755×10^{-2}
Y_H	0.0000×10^{-0}	0.0000×10^{-0}	2.7105×10^{-4}
Y_{OH}	0.0000×10^{-0}	0.0000×10^{-0}	1.4821×10^{-2}
Y_O	0.0000×10^{-0}	0.0000×10^{-0}	1.7807×10^{-3}
Y_{H_2}	2.8522×10^{-2}	2.8522×10^{-2}	2.5670×10^{-3}
Y_{H_2O}	0.0000×10^{-0}	0.0000×10^{-0}	2.2166×10^{-1}
Y_{HO_2}	0.0000×10^{-0}	0.0000×10^{-0}	2.2350×10^{-5}
$Y_{H_2O_2}$	0.0000×10^{-0}	0.0000×10^{-0}	3.0765×10^{-6}
Y_{N_2}	7.4512×10^{-1}	7.4512×10^{-1}	7.4512×10^{-1}
X_{O_2}	1.4793×10^{-1}	1.4793×10^{-1}	1.0269×10^{-2}
X_H	0.0000×10^{-0}	0.0000×10^{-0}	6.4243×10^{-3}
X_{OH}	0.0000×10^{-0}	0.0000×10^{-0}	2.0818×10^{-2}
X_O	0.0000×10^{-0}	0.0000×10^{-0}	2.6589×10^{-3}
X_{H_2}	2.9586×10^{-2}	2.9586×10^{-2}	3.0421×10^{-2}
X_{H_2O}	0.0000×10^{-0}	0.0000×10^{-0}	2.9395×10^{-1}
X_{HO_2}	0.0000×10^{-0}	0.0000×10^{-0}	1.6177×10^{-5}
$X_{H_2O_2}$	0.0000×10^{-0}	0.0000×10^{-0}	2.1607×10^{-6}
X_{N_2}	5.5621×10^{-1}	5.5621×10^{-1}	6.3544×10^{-1}

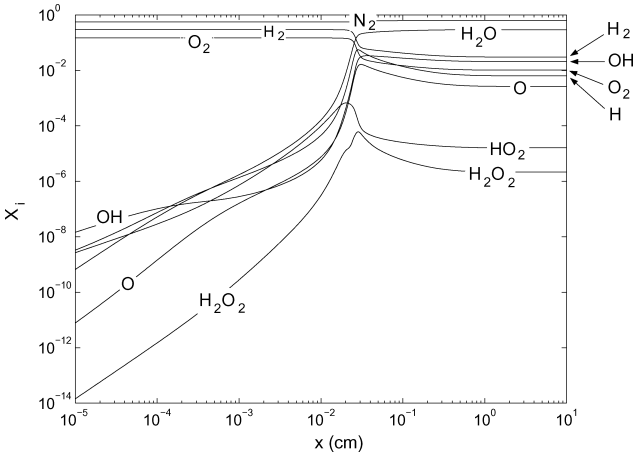

Fig. 1 Species mole fraction vs distance.

Values of various thermochemical and dynamic properties at the initial state, shock state, and equilibrium state are given in Table 2. Here, to allow comparison with Refs. 9 and 10, mole fractions, in addition to mass fractions are reported. The simulations to be shown, with the exception of one in which p_0 is varied, are performed at the conditions of Table 2.

Figure 1 shows the spatial distribution of species mole fractions throughout the reaction zone. This calculation was performed with the Adams implicit method embodied in DLSODE. Results can be directly compared to those of Shepherd, who reports predictions over the reaction zone length scale whose structures can be discerned down to the induction zone length scale, but not at the finest scales. The use of log–log scaling in Fig. 1 reveals a variety of scales over which the mole fractions evolve. The shock front is located at $x = 0$ cm. Just past the shock, collisions of the major species H_2, O_2, and N_2 commence with more vigor, and minor species are generated. For very small distances from the shock front $0 < x < 10^{-4}$ cm, the mole fractions of minor species H, O, OH, H_2O, HO_2, and H_2O_2 grow at rates that are well modeled by power laws, whereas major species mole fractions are essentially unchanged. Power law variation, that is, $X_i \sim x^{\alpha}$, where α is a real constant, is rigorously demonstrated in Ref. 10 in the related time domain at early time. Such a variation is represented as a straight line with slope α in log–log plots such as Fig. 1; were the scale of the x axis extended to even finer scales formally admitted by the continuum assumption, the slope would remain constant.

At $x \sim 10^{-4}$ cm, one notices the slopes of some of the curves, for example, that for OH, begin to change; this suggests that, at this scale, significant molecular collisions at the mean free path length scale are inducing chemical reactions of the minor species. For $10^{-4} < x < 10^{-2}$ cm, major species collisions continue, minor species mole fractions continue to grow rapidly, and the minor species continue to interact. Just past $x = 10^{-2}$ cm, a particularly vigorous stage of the reaction ensues in which all species mole fractions, except the inert N_2, undergo significant change. This region is considered to be near the end of the induction zone, whose boundary is defined in the standard fashion by the point at which the temperature gradient $\mathrm{d}T/\mathrm{d}x$ reaches a maximum value. With this definition, the induction zone thickness is found to be 2.6×10^{-2} cm. It is also the beginning of the thermal explosion zone, which extends from roughly $2.6 \times 10^{-2} < x < 3 \times 10^{-2}$ cm. This is followed by a relatively long recombination zone, $3 \times 10^{-2} < x < 10^{0}$ cm, in which radicals recombine exothermically into the predominant product specie, H_2O. For $x > 10^{0}$ cm, it is clear from Fig. 1 that the system has come to an equilibrium because all spatial gradients are near zero. This is confirmed by calculating the equilibrium state with an iterative Newton solver for $f_i(Y_1, \ldots, Y_{N-L}) = 0$.

Temperature and pressure in the reaction zone are shown in Figs. 2 and 3, respectively. In Figs. 2 and 3, the induction zone is clearly shown as a region of essentially constant temperature and pressure. This seeming tranquility masks the real underlying evolution of species mole fractions that is occurring within this zone. In contrast, the variation of pressure and temperature in the recombination zone is mild in comparison.

The multiscale nature of the problem is most clearly shown in Fig. 4. Here the length scales $\ell_i(x)$ predicted by the local eigenvalue analysis described earlier are shown as functions of the distance from the shock. Each curve corresponds to the reciprocal of the absolute value of the real part of an eigenvalue. Most important, the finest length scale is seen to vary from near 10^{-4} cm in the induction zone to as low as 2.3×10^{-5} cm in the recombination zone. The variation of mole fractions on these fine scales is present throughout the entire reaction zone. Because the mole fractions in Fig. 1 are the result of the local linear combination of all eigenmodes, one only discerns

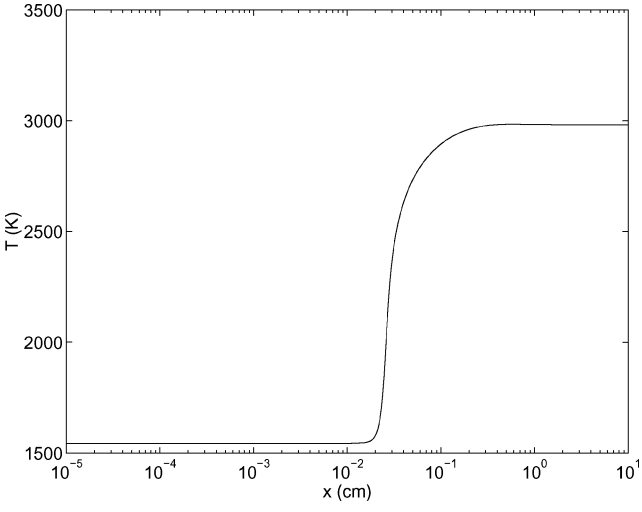

Fig. 2 Temperature vs distance.

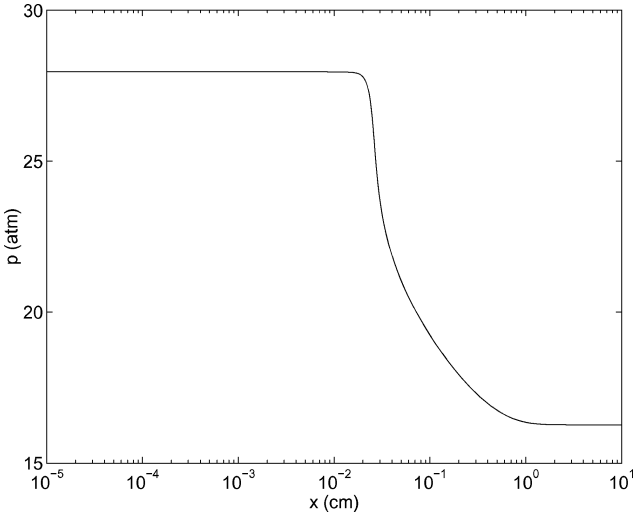

Fig. 3 Pressure vs distance.

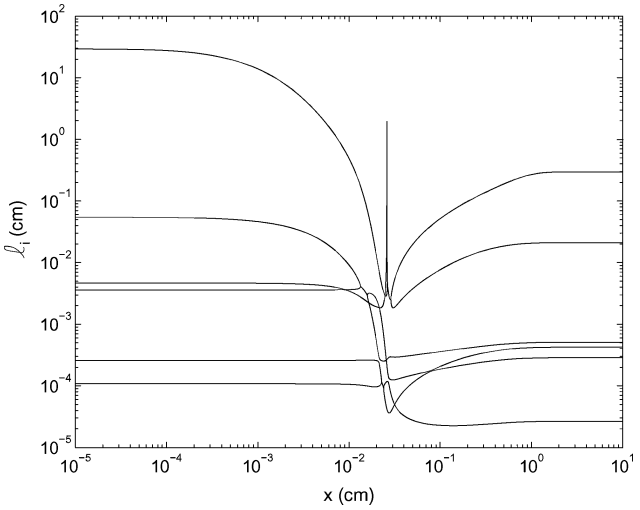

Fig. 4 Length scales vs distance.

the fine-scale effects in the minor species mole fractions in the near-shock region, $x \sim 10^{-4}$ cm.

The finest scales are likely close to mean free path length scales, and thus, this continuum calculation is probably approaching its lower limit of validity. In fact, a simple independent Navier–Stokes calculation of a comparable inert viscous shock structure reveals that the viscous length scales are precisely the same order of magnitude as the finest reaction length scales. This is likely a consequence of both constitutive models for reaction and diffusion having molecular collisions as their causal mechanism,[35,36] thus inducing all transport and reaction constitutive models to yield the same mean free path-limited finest length scale. Note that the present analysis serves to correct a speculation made in Ref. 20, where it was inferred, from a timescale analysis that did not include a detailed consideration of species convection, that length scales would be predicted that would give rise to a violation of the continuum assumption.

The largest length scales range from around 3×10^1 cm in the induction zone to around 3×10^{-1} cm at equilibrium state. The smallest length scale is consistent with the smallest scale on which mole fractions are seen to vary in Fig. 1. Moreover, the smallest scale is roughly equal to the internal step size utilized by the adaptive DLSODE integration subroutine, in which the size of the integration step is automatically chosen to maintain stability as well as achieve the specified accuracy. The largest length scale is not as critical, but does provide a useful estimate of the overall length of the reaction zone.

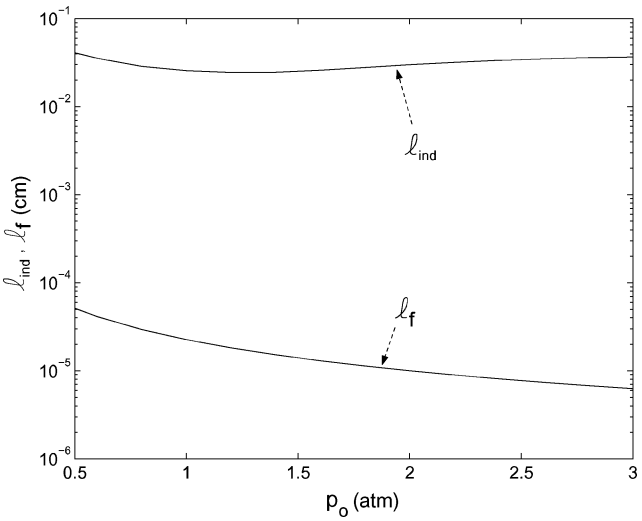

Fig. 5 Induction zone length and finest length scale vs initial pressure.

Additional features of Fig. 4 are noteworthy. For the bulk of the domain, there are $N–L = 6$ real and distinct eigenvalues. For $x < 3 \times 10^{-2}$ cm, five of these eigenvalues have negative real parts, and one has a positive real part, indicating growth of a local eigenmode. For $x > 3 \times 10^{-2}$ cm, the real parts of all six eigenvalues are negative, indicating a relaxation to equilibrium. The spike in one of the curves near $x = 3 \times 10^{-2}$ cm indicates one of the eigenvalues has a real part passing through zero; hence, its reciprocal approaches infinity. In a few isolated regions near the end of the induction zone and in the thermal explosion zone, some of the eigenvalues are complex conjugates. This is indicative of a local oscillatory behavior and is seen in Fig. 4 when some of the curves merge in a thin zone. Whereas a few curves appear to cross, a fine-scale calculation shows that they in fact remain distinct, even when up to three orders of magnitude increase in resolution is employed.

B. Effect of Initial Pressure

A series of calculations in the same mixture held at the same initial temperature was performed in which the initial pressure varied from 0.5 to 3.0 atm. Again, detonations that were very near to the CJ state were studied, and both the finest length scale given by the eigenvalue analysis as well as the induction length scale were predicted. Results are summarized in Fig. 5. Here it is clearly demonstrated that the smallest length scale is roughly three orders of magnitude finer than that of the induction zone. The predictions of the induction zone length compare well with those given in Ref. 11, where the same physical problem was modeled with a slightly different kinetics model.

C. Verification

Two types of verification of the predictions are given here: 1) a comparison to Mikolaitis's[10] detailed induction zone predictions and 2) a formal grid convergence study. For the first verification, some small adjustments are necessary. In Ref. 10, only the induction zone was considered, and p, T, and u were frozen at their postshock values. Then the governing equations were integrated numerically in time and results compared favorably to those of a detailed asymptotic theory. To compare predictions properly, the time coordinate of a Lagrangian particle must be obtained by numerical integration of the equation for particle velocity, $u = \mathrm{d}x/\mathrm{d}t$. Because $u(x)$ is available after solution of Eq. (56), the local time can be found by the quadrature

$$t = \int_0^x \frac{\mathrm{d}\hat{x}}{u(\hat{x})} \tag{65}$$

Here, $\hat{x}$ is a dummy variable. When this result is used, it is then possible to plot the variation of all thermochemical properties of

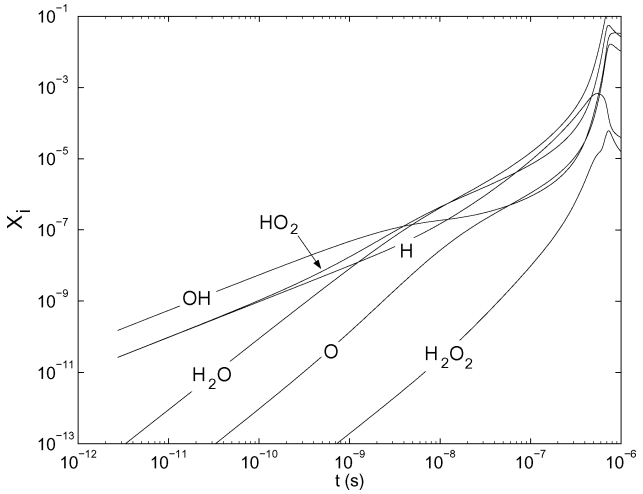

Fig. 6 Minor species mole fractions vs time in the induction zone.

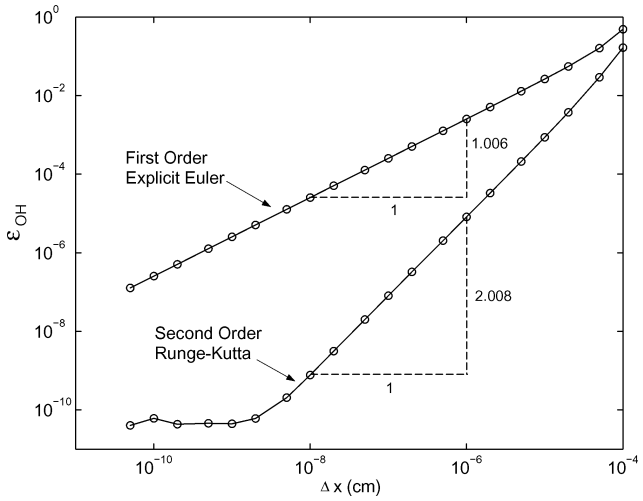

Fig. 7 Relative error in X_{OH} at $x = 1 \times 10^{-4}$ cm as a function of discretization scale Δx.

a fluid particle as a function of the relative time after which it has passed the shock located at $x = 0$. Such a plot is given in Fig. 6 for the mole fractions of all species in the induction zone. The features are roughly the same as those seen in Fig. 6. A direct comparison to the predictions of Ref. 10 shows excellent agreement for all variables.

For the second verification, a formal grid convergence study is performed over a wide range of spatial discretization levels: $5 \times 10^{-11} < \Delta x < 10^{-4}$ cm. Whereas the finest discretization scales are definitely below the continuum limit, for purposes of mathematical verification of the numerical method, this is inconsequential. Conditions were identical to those used to predict Fig. 1. Because it was desirable to use a fixed value of Δx in an individual calculation, use of the adaptive DLSODE was discarded in favor of a simpler first-order explicit Euler and second-order explicit Runge–Kutta method. Although both of these methods work well over the entire reaction zone, it was more efficient to determine the convergence properties by integrating only to a small final value of distance, here taken to be $x = 10^{-4}$ cm. Because this final value of x is as small as the finest length scale, it is guaranteed there will be no problems with numerical stability.

Figure 7 shows the results of the grid convergence study. First, results were obtained on a highly refined grid with $\Delta x = 10^{-11}$ cm for the second-order method. These were taken as a benchmark solution to which comparisons could be made. Next, it was chosen to compare the mole fraction values of a minor species X_{OH}, at the final point $x = 10^{-4}$ cm to the prediction of the benchmark case. For each discretization and integration method, a value of the relative error ε_{OH}

$$\varepsilon_{OH} = \left| \frac{X_{OH,\ \text{approximate}} - X_{OH,\ \text{benchmark}}}{X_{OH,\ \text{benchmark}}} \right|_{x = 10^{-4}\ \text{cm}}$$

was calculated. Had other variables been chosen or an error norm encompassing a broader domain been chosen, the convergence rates would not have been affected.

The first-order Euler method in fact gives error predictions that converge at a rate of 1.006, effectively equivalent to its expected value. At the smallest $\Delta x = 5 \times 10^{-11}$ cm studied, the method is still converging and has not yet reached its machine roundoff limit. The second-order Runge–Kutta method predicts errors to converge at a rate of 2.008, again equivalent to its expected value. Its error is always lower than that of the first-order method, and near $\Delta x = 2 \times 10^{-9}$ cm, it appears that the machine roundoff limit has been reached as further refinement results in no improvement in the error. The actual relative error at this limit is just under 10^{-10}, which indicates that the accuracy exceeds that of single precision. It is likely that the strict double precision limit of 10^{-16} is not reached because of the effects of accumulation of roundoff error after many millions of operations.

D. Numerical Stability

A series of calculations was subsequently performed at discretization levels near the threshold of numerical instability. Conditions again were identical to those used to predict Fig. 1. Figure 8 shows predictions of X_H over the range $0 < x < 5 \times 10^{-3}$ cm using a first-order explicit Euler integration. Similar results could have been obtained for other variables or using other integration schemes; it is difficult, however, for the subroutine DLSODE to generate spatially unstable numerical results because it uses automatic step size selection to prevent this from happening. Thus, in effect DLSODE is providing an atypical adaptive mesh refinement. In more challenging spatiotemporal problems, multiscale effects often require adaptation in space and time. In such cases, solvers like DLSODE are confined to adaptation in time; independent algorithms, such as the wavelet adaptive multilevel representation,[20] are required to address the multiscaled spatial structures. This extension to adaptation in space and time is nontrivial.

For a value of $\Delta x = 1.00 \times 10^{-5}$ cm, well below the finest physical length scale predicted by the eigenvalue analysis, the evolution of X_H is well-behaved. Increasing Δx to a value in the neighborhood of the smallest physical length scale, $\Delta x = 2.00 \times 10^{-4}$ cm, results in a prediction that is oscillatory but stable. Increasing the discretization length slightly to $\Delta x = 2.38 \times 10^{-4}$ cm triggers an unstable numerical oscillation.

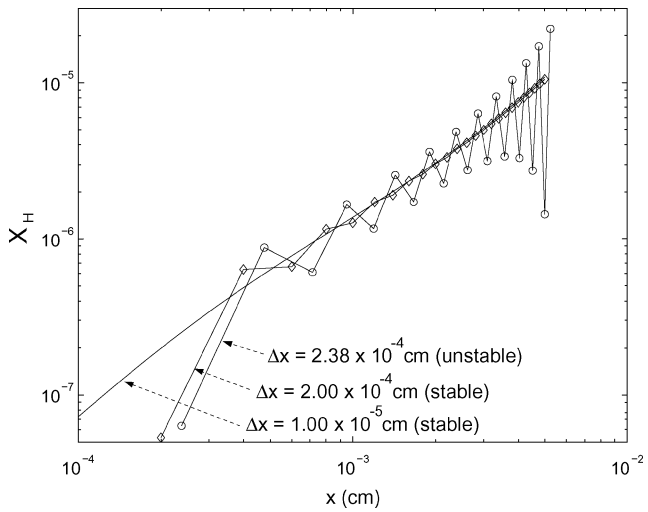

Fig. 8 X_H vs x in the near-shock region using with first-order explicit Euler method.

If one were to model a similar detonation using a computational model that allowed for both time and space variation and one were to choose a computational grid that did not capture the finest physical length scale, the following result would be likely. In the steady-state limit, the model would be inclined to predict relaxation to a spatially oscillatory state similar to that shown in the large Δx case of Fig. 8. Such oscillations are damped, however, in the unsteady model by artificial diffusion, which depends on both the grid and computational algorithm employed. This may account for the wide disparity in the small-scale structures that one often sees in predictions of identical cases by either the same algorithm on different grids, different algorithms on the same grid, or even the same algorithm and same grid on different computers. A good discussion of how grid- and algorithm-dependent numerical diffusion arises for various numerical methods for hyperbolic systems of equations is given by LeVeque.[37]

E. Comparison with Recent Results

Finally, predictions of the current algorithm are compared with some of the best calculations of detonations in hydrogen-based systems that have appeared in the recent archival literature. In all cases, these calculations give predictions that have no obvious macroscale errors. The results are summarized in Table 3, which lists the induction zone length ℓ_{ind}, the finest length predicted by the eigenvalue analysis ℓ_f, and the grid discretization Δx employed in the study. Unless otherwise indicated in Table 3, parameters are inferred from those reported by the original authors and are for CJ detonations. For each case, the algorithm presented here was exercised on the published models under the appropriate conditions reported. In addition, when available, ℓ_{ind} as reported in the cited sources is listed. The induction length scale obtained for the low-pressure $2H_2 + O_2 + 7Ar$ case agrees within 11 and 9% to the results reported, respectively, in Refs. 15 and 13, but not with that reported in Ref. 12. It is believed that the value reported in Ref. 12 (2×10^{-3} cm) is a typographical error because agreement is obtained with other reported values from Ref. 12. The induction zone length predicted in Ref. 20 differs by a factor of three with that of the present study. Possible causes for this discrepancy are that in Ref. 20 diffusion was included, a looser definition of ℓ_{ind} was employed, and not all of the fine-scale reaction lengths were fully resolved. However, the key results found in Table 3 are 1) none of these independent studies has captured ℓ_f, most employ grids whose finest scale is orders of magnitude larger than ℓ_f, and 2) the capture of ℓ_{ind} is at best not precise, some have the proper order of magnitude, whereas others again have grids whose finest scale is much larger than ℓ_{ind}. Whereas these are some of the best calculations, it is not difficult to find worse cases in the literature.

One may legitimately question why the underresolved detonation calculations just described produce results that in some regards seem to be intuitively correct. The following hypotheses are offered. First, the intuition of many practitioners has its foundation in equilibrium thermodynamics. Properties such as final temperature, pressure, species concentrations, and wave speed, at least in one-dimensional steady calculations, are not strongly linked to the details of the reaction zone structure, and so it is entirely possible to calculate an incorrect structure that relaxes to the correct equilibrium. Also in that numerical diffusion, inherent in all calculations with time and space dependency, serves to suppress the instabilities that underresolved steady calculations exhibit (Fig. 8), the influence of underresolution is often not obvious.

Second, whereas the actual macroscale effects of underresolution in a specific unsteady calculation remain to be shown, it is not difficult to speculate on physical scenarios in which problems might arise. Three are considered here: 1) It is likely that a precise prediction of the induction zone length requires a proper resolution of those causal fine-scale phenomena that trigger this highly nonlinear event. One does not find in the literature systematic grid convergence studies for the induction zone length, and so it is difficult to say how well the physics have been captured. 2) For detonations with curvature, new geometric length scales are introduced that compete with the reaction zone length scales in determining overall wave dynamics. Correctly capturing the speeds of detonations diffracting in a multidimensional environment hinges on correctly representing the physics of the reaction zone length scales and curvature length scales. 3) In any unsteady calculation, a Fourier decomposition of any transient detonation will have high wave number modes whose wavelength is the same order of magnitude as the finest scales in the steady structure. In many cases, the high wave number modes tend to be stable, but one can envision cases in which unstable modes exist whose wavelength is of the same order of magnitude as the finest length scales of the steady system. In any case, and especially in unstable cases, fully capturing the unsteady dynamics demands that length scales at or below the finest steady length scale be examined. Otherwise numerical viscosity may be suppressing a true physical instability.

Table 3 Comparison of length scales among various models that use detailed kinetics to describe detonations in hydrogen-based systems

Ref.	Mixture	T_0, K	p_0, atm	ℓ_{ind}, cm: Present study	ℓ_{ind}, cm: Reported value	ℓ_f, cm	Δx, cm
12	$2H_2 + O_2 + 7Ar$	2.98×10^2	6.58×10^{-2}	1.47×10^{-1}	2.00×10^{-3}	2.17×10^{-4}	3.88×10^{-3}[a]
13	$2H_2 + O_2 + 7Ar$	2.98×10^2	6.58×10^{-2}	1.47×10^{-1}	1.60×10^{-1}	2.17×10^{-4}	2.50×10^{-3}
15	$2H_2 + O_2 + 7Ar$	2.98×10^2[b]	6.61×10^{-2}	1.46×10^{-1}	1.30×10^{-1}	——[c]	——[d]
16	$2H_2 + O_2$[e]	2.92×10^2	2.45×10^{-1}	2.35×10^{-2}	——	4.74×10^{-5}	8.20×10^{-3}[f]
18	$2H_2 + O_2 + 3.76N_2$[g]	2.98×10^2[b]	1.00×10^0[b]	1.50×10^{-2}	——	1.23×10^{-5}	5.00×10^{-4}[a]
19	$2H_2 + O_2 + 3.76N_2$[h]	3.00×10^2	8.39×10^{-1}	2.82×10^{-2}	——	2.82×10^{-5}	1.00×10^{-2}[i]
20	$2H_2 + O_2 + 7Ar$	1.20×10^3	1.17×10^0	1.54×10^{-2}	4.70×10^{-2}	2.76×10^{-5}	8.14×10^{-5}[j]
21	$2H_2 + O_2 + 7Ar$	1.20×10^3	1.17×10^0	1.54×10^{-2}	——	2.76×10^{-5}	3.00×10^{-2}
22	$2H_2 + O_2$	3.00×10^2	1.00×10^0	5.30×10^{-3}	——	7.48×10^{-6}	1.00×10^{-2}[a]
23	$2H_2 + O_2 + 3.76N_2$	9.00×10^2	2.27×10^{-1}	1.38×10^{-1}[k]	——	2.23×10^{-4}[k]	1.00×10^0[f]
24	$2H_2 + O_2 + 3.76N_2$[h]	3.00×10^2	2.50×10^1	1.80×10^{-2}	——	5.61×10^{-7}	5.94×10^{-2}

[a] Smallest discretization considered.
[b] Value not explicitly reported, but presumed.
[c] Intrinsic low-dimensional manifold used, finest scale not obvious.
[d] Adaptive mesh refinement method used, grid size not obvious.
[e] CJ adopted; original study employs underdrive.
[f] Rough estimate from parameters provided.
[g] Presumed stoichiometric; detonation overdriven at $D = 2.065 \times 10^5$ cm.
[h] CJ adopted; original study employs overdrive.
[i] Adaptive mesh refinement used with three levels of refinement; grid size estimated.
[j] Adaptive mesh refinement method used with 16 levels of refinement.
[k] Effects of nitrogen chemistry neglected in estimate.

V. Conclusions

It has been unambiguously shown that the finest length scales predicted by a one-dimensional steady analysis of a common stoichiometric CJ hydrogen–air detonation model under standard atmospheric conditions are roughly three orders of magnitude finer than the induction zone thickness. Consequently, many modern calculations using detailed kinetics coupled with a strategy to resolve at most the induction zone are formally underresolved. Moreover, the precise calculation of the induction zone thickness likely requires a proper resolution of the fine-scale structures that constitute the induction zone. It is also clear that to meet the strictest demands of rigorous scientific computing for detonations with detailed kinetics, one must employ a computational grid with a characteristic length at or below the values predicted by the present analysis. In fact when other physics is considered, such as detonations with curvature,[5] or those in which high wave number instabilities are present,[6] the demands of spatial resolution may be even more stringent than those suggested here. Furthermore, because preliminary calculations indicate the finest reaction zone length scales are of the same order as diffusion length scales in shocks, it is likely the case that a physically consistent resolved model of detonation that includes detailed kinetics needs also to consider diffusion. This is because constitutive theories for detailed kinetics and mass, momenta, and energy diffusion are representations of the same molecular collision-based phenomena.

That underresolved computations often produce plausible results is understandable when one considers that a wide variety of calculations are driving toward a stable equilibrium state that is fixed by path-independent thermodynamics. It is often the case that these near-equilibrium properties are the easiest to predict as well as observe. However, for many classes of problems, such as those with inherent unsteadiness, the journey is as important as the destination, and agreement with equilibrium wave speeds, pressures, and temperatures is a necessary but insufficient requirement. In such cases, the journey is only properly completed when the spatial structures are properly resolved. Short cuts to equilibrium provided by underresolved paths do not reflect the full richness of the process and run the risk of leading the journey to a nonphysical catastrophe.

It is often argued that such fine discretizations are not necessary because the small scales will not influence the scales of engineering importance. First, such a conclusion cannot be made a priori; indeed, the field of nonlinear dynamics provides many counterexamples in which small-scale disturbances ultimately manifest themselves on a large scale. Lorenz's[38] now-celebrated study of transition to chaos is but one such case. Thus, until such calculations are actually made that prove the unimportance of small scales, the possibility of their relevance cannot be cavalierly dismissed. Second, if it is indeed the case that these small scales are of no consequence, then it is appropriate for the modeling community to employ only mathematical models that do not contain such inherently fine scales. To argue on one hand that it is critical that modern engineering applications require a consideration of detailed chemical kinetics and on the other hand that fine-scale phenomena are of no consequence is scientifically incoherent. That said, the present study is incapable of answering the critical question of how important the fine-scale structures are. It just provides a simple diagnosis that most computational combustion results in the literature are afflicted with underresolution. The prognosis, however, can still be bright but only if a careful regimen of detailed, resolved calculations of key physical problems, transparently presented so that a skeptical broader community can have full confidence in the predictions, is undertaken.

References

[1]Roache, P. J., "Quantification of Uncertainty in Computational Fluid Dynamics," *Annual Review of Fluid Mechanics*, Vol. 29, 1997, pp. 123–160.

[2]Roache, P. J., "Verification of Codes and Calculations," *AIAA Journal*, Vol. 36, No. 5, 1998, pp. 696–702.

[3]Oberkampf, W. L., and Blottner, F. G., "Issues in Computational Fluid Dynamics Code Verification and Validation," *AIAA Journal*, Vol. 36, No. 5, 1998, pp. 687–695.

[4]Oberkampf, W. L., and Trucano, T. G., "Verification and Validation in Computational Fluid Dynamics," *Progress in Aerospace Sciences*, Vol. 38, No. 3, 2002, pp. 209–272.

[5]He, L., "Theoretical Determination of the Critical Conditions for the Direct Initiation of Detonations in Hydrogen–Oxygen Mixtures,"' *Combustion and Flame*, Vol. 104, No. 4, 1996, pp. 401–418.

[6]Short, M., and Sharpe, G. J., "Pulsating Instability of Detonations with a Two-Step Chain-Branching Reaction Model: Theory and Numerics," *Combustion Theory and Modelling*, Vol. 7, No. 2, 2003, pp. 401–416.

[7]Fickett, W., and Davis, W. C., *Detonation*, Univ. of California Press, Berkeley, CA, 1979, Chap. 5.

[8]Westbrook, C. K., "Hydrogen Oxidation Kinetics in Gaseous Detonations," *Combustion Science and Technology*, Vol. 29, Nos. 1–2, 1982, pp. 67–81.

[9]Shepherd, J. E., "Chemical Kinetics of Hydrogen–Air–Diluent Detonations," *Dynamics of Explosions*, edited by J. R. Bowen, J.-C. Leyer, and R. I. Soloukhin, Vol. 106, Progress in Astronautics and Aeronautics, AIAA, New York, 1986, pp. 263–293.

[10]Mikolaitis, D. W., "An Asymptotic Analysis of the Induction Phases of Hydrogen–Air Detonations," *Combustion Science and Technology*, Vol. 52, Nos. 4–6, 1987, pp. 293–323.

[11]Lu, T., Law, C. K., and Ju, Y., "Some Aspects of Chemical Kinetics in Chapman–Jouguet Detonation: Induction Length Analysis," *Journal of Propulsion and Power*, Vol. 19, No. 5, 2003, pp. 901–907.

[12]Oran, E. S., Weber, J. W., Stefaniw, E. I., Lefebvre, M. H., and Anderson, J. D., "A Numerical Study of a Two-Dimensional H_2–O_2–Ar Detonation Using a Detailed Chemical Reaction Model," *Combustion and Flame*, Vol. 113, Nos. 1–2, 1998, pp. 147–163.

[13]Hu, X. Y., Khoo, B. C., Zhang, D. L., and Jiang, Z. L., "The Cellular Structure of a Two-Dimensional $H_2/O_2/Ar$ Detonation Wave," *Combustion Theory and Modelling*, Vol. 8, No. 2, 2004, pp. 339–359.

[14]Eckett, C. A., Quirk, J. J., and Shepherd, J. E., "The Role of Unsteadiness in Direct Initiation of Gaseous Detonations," *Journal of Fluid Mechanics*, Vol. 421, 2000, pp. 147–183.

[15]Pintgen, F., Eckett, C. A., Austin, J. M., and Shepherd, J. E., "Direct Observations of Reaction Zone Structure in Propagating Detonations," *Combustion and Flame*, Vol. 133, No. 3, 2003, pp. 211–229.

[16]Sheffer, S. G., Martinelli, L., and Jameson, A., "An Efficient Multigrid Algorithm for Compressible Reactive Flows," *Journal of Computational Physics*, Vol. 144, No. 2, 1998, pp. 484–516.

[17]Sheffer, S. G., Martinelli, L., and Jameson, A., "Simulation of Reacting Hydrocarbon Flows with Detailed Chemistry," *Combustion Science and Technology*, Vol. 136, Nos. 1–6, 1998, pp. 55–80.

[18]Tsuboi, N., Katoh, S., and Hayashi, A. K., "Three-Dimensional Numerical Simulation for Hydrogen/Air Detonation: Rectangular and Diagonal Structures," *Proceedings of the Combustion Institute*, Vol. 29, 2002, pp. 2783–2788.

[19]da Silva, L. F. F., Azevedo, J. L. F., and Korzenowski, H., "Unstructured Adaptive Grid Flow Simulations of Inert and Reactive Gas Mixtures," *Journal of Computational Physics*, Vol. 160, No. 2, 2000, pp. 522–540.

[20]Singh, S., Rastigejev, Y., Paolucci, S., and Powers, J. M., "Viscous Detonation in H_2–O_2–Ar Using Intrinsic Low-Dimensional Manifolds and Wavelet Adaptive Multilevel Representation," *Combustion Theory and Modelling*, Vol. 5, No. 2, 2001, pp. 163–184.

[21]Fedkiw, R. P., Merriman, B., and Osher, S., "High Accuracy Numerical Methods for Thermally Perfect Gas Flows with Chemistry," *Journal of Computational Physics*, Vol. 132, No. 2, 1997, pp. 175–190.

[22]Ebrahimi, H. B., and Merkle, C. L., "Numerical Simulation of a Pulse Detonation Engine with Hydrogen Fuels," *Journal of Propulsion and Power*, Vol. 18, No. 5, 2002, pp. 1042–1048.

[23]Dudebout, R., Sislian, J. P., and Oppitz, R., "Numerical Simulation of Hypersonic Shock-Induced Combustion Ramjets," *Journal of Propulsion and Power*, Vol. 14, No. 6, 1998, pp. 869–879.

[24]Choi, J.-Y., Jeung, I.-S., and Yoon, Y., "Numerical Study of Scram Accelerator Starting Characteristics," *AIAA Journal*, Vol. 36, No. 6, 1998, pp. 1029–1038.

[25]He, X., and Karagozian, A. R., "Numerical Simulation of Pulse Detonation Engine Phenomena," *Journal of Scientific Computing*, Vol. 19, Nos. 1–3, 2003, pp. 201–224.

[26]Sichel, M., Tonello, N. A., Oran, E. S., and Jones, D. A., "A Two-Step Kinetics Model for Numerical Simulation of Explosions and Detonations in H_2–O_2 Mixtures," *Proceedings of the Royal Society of London, Series A: Mathematical and Physical Sciences*, Vol. 458, No. 2017, 2002, pp. 49–82.

[27]Kawai, S., and Fujiwara, T., "Numerical Analysis of First and Second Cycles of Oxyhydrogen Pulse Detonation Engine," *AIAA Journal*, Vol. 41, No. 10, 2003, pp. 2013–2019.

[28]Korobeinikov, V. P., Levin, V. A., Markov, V. V., and Chernyi, G. G., "Propagation of Blast Waves in a Combustible Gas," *Astonautica Acta*, Vol. 17, Nos. 4–5, 1972, pp. 529–537.

[29]Whitham, G. B., *Linear and Nonliner Waves*, Wiley, New York, 1974, pp. 113–117.

[30]Strang, G., *Linear Algebra and its Applications*, 3rd ed., Harcourt Brace Jovanovich, Fort Worth, TX, 1988, pp. 275–277.

[31]Kee, R. J., Rupley, F. M., and Miller, J. A., "Chemkin-II: A Fortran Chemical Kinetics Package for the Analysis of Gas Phase Chemical Kinetics," Sandia National Labs., Rept. SAND89-8009B, Livermore, CA, Nov. 1991.

[32]Kee, R. J., Rupley, F. M., and Miller, J. A., "The Chemkin Thermodynamic Data Base," Sandia National Labs., Rept. SAND87-8215B, Livermore, CA, March 1990.

[33]Hindmarsh, A. C., "ODEPACK, a Systematized Collection of ODE Solvers," *Scientific Computing*, edited by R. S. Stepleman, et al., North-Holland, Amsterdam, 1983, pp. 55–64.

[34]Miller, J. A., Mitchell, R. E., Smooke, M. D., and Kee, R. J., "Toward a Comprehensive Chemical Kinetic Mechanism for the Oxidation of Acetylene: Comparison of Model Predictions with Results from Flame and Shock Tube Experiments," *Proceedings of the Nineteenth Symposium (International) on Combustion*, Combustion Inst., Pittsburgh, PA, 1982, pp. 181–196.

[35]Hirschfelder, J. O., Curtis, C. F., and Bird, R. B., *Molecular Theory of Gases and Liquids*, Wiley, New York, 1954, pp. 441–667.

[36]Laidler, K. J., *Chemical Kinetics*, McGraw–Hill, New York, 1965, pp. 63–68.

[37]LeVeque, R. J., *Finite Volume Methods for Hyperbolic Problems*, Cambridge Univ. Press, Cambridge, England, U.K., 2002, pp. 151–155.

[38]Lorenz, E. N., "Deterministic Nonperiodic Flow," *Journal of the Atmospheric Sciences*, Vol. 20, March 1963, pp. 130–141.

C. Kaplan
Associate Editor